Hindawi
Shock and Vibration
Volume 2022, Article ID 1546622, 19 pages
https://doi.org/10.1155/2022/1546622

Research Article

Three-Level SOC Equalization Control Strategy for MMC-BESS Based on Feedforward Sliding Window Integral Method

Yuan Cheng,[1,2] Hui Zhang ,[1] Xiaohui Wei,[3] and Wenquan Shao[2]

[1]*School of Electrical Engineering, Xi' an University of Technology, Xi' an 710048, China*
[2]*School of Electronics Information, Xi'an Polytechnic University, Xi'an 710048, China*
[3]*Xi'an Electric Power Supply Company of State Grid Shaanxi Electric Power Company, Xi'an 710032, China*

Correspondence should be addressed to Hui Zhang; zhangh@xaut.edu.cn

Received 10 December 2021; Revised 31 May 2022; Accepted 2 June 2022; Published 20 September 2022

Academic Editor: Liu Jing

The modular multilevel converter of the battery energy storage system (MMC-BESS) not only is suitable for the large-scale energy storage and dispatching of AC and DC grids, but also has a strong ability to suppress power fluctuations caused by the new energy output or grid failures. When an asymmetric voltage or a sudden change in DC load occurs in the AC grid, in order to compensate for the power difference between AC and DC sides, the energy storage submodule of the MMC-BESS will have a large unbalanced charging and discharging current, destroying the equalization state of SOC and seriously affecting energy storage capacity utilization and battery service life. In order to deal with the above problems, in this paper, the characteristics of the power difference between the MMC-BESS phase unit and the upper and lower bridge arms are analyzed. It is found that when considering the fluctuation of the submodule capacitor voltage, the phase unit power has the fundamental frequency AC circulating current component, and the power difference between the upper and lower bridge arms has the DC circulating current component. Therefore, the three-level SOC equalization correction control strategy is proposed based on interphase, upper and lower bridge arms, and submodules, and the feedforward sliding window integral method is introduced into the SOC equalization correction control layer of upper and lower bridge arms, so as to achieve the purpose of more balanced and accurate power distribution among phases and among upper and lower bridge arms of each phase. The simulation results show that the MMC-BESS has effective compensation ability when there is a large power difference in the AC and DC power grid. Under the unbalanced working conditions of the three-phase power grid, the three-phase AC current can quickly reach equalization, and the total harmonic content is 1.38%, and the unbalance degree is 2.4%. Under the same operating conditions, compared with the traditional optimal one-third average method, the SOC equalization correction control strategy proposed in this paper has smaller submodule capacitor voltage fluctuation rate, harmonic distortion rate, and three-phase system circulating current. And the SOC of each phase has a faster equalization convergence speed.

1. Introduction

In recent years, with the large-scale access of new energy resources, the randomness of its power flow has brought severe challenges to the safe and stable operation of the power grid [1]. In the case of power quality problems mainly due to voltage sag [2] caused by uneven output of new energy sources or sudden load changes in the AC and DC grids, the energy storage system, as a balance medium between power and time scale, can not only buffer the power fluctuation caused by new energy power generation, but also effectively improve the power quality of the power grid [3–5].

Modular multilevel converters are currently widely used in high-voltage DC transmission, new energy power generation, and other medium-high-voltage and large-capacity occasions due to their highly modular structure, low harmonic content of AC output, and strong redundancy [6, 7]. Combining the MMC with the lithium battery, which has high energy density, high power density, and high energy conversion efficiency [8], can give full play to the ability of the MMC-BESS to adjust power quality and smooth power

fluctuation output in medium and high power occasions [9–11].

In AC and DC power grids, the unbalanced grid-side voltage of the three-phase or the large sudden change of AC and DC load makes the system bus voltage unstable and increases the system circulating current, which causes damage to electrical products, misoperation of power grid protection, and reduces the service life of distribution grid operation equipment, etc. [12, 13]. The use of the large-capacity MMC-BESS can supplement the power difference between the AC and DC sides, smooth power fluctuations, and improve the system power quality [14, 15]. However, when the battery in the MMC-BESS is in use, long-term unbalanced high current charging and discharging will affect its SOC equalization state and energy storage capacity utilization, resulting in a decrease in battery life [16].

Therefore, it is essential to carry out the research on the SOC equalization control of the MMC-BESS. Literature [17] used zero-sequence voltage and fundamental frequency circulating current injection to achieve the SOC balance among phases and among upper and lower bridge arms, but the calculation principle is complicated. Literature [18] introduced the energy storage MMC system in which the energy storage battery was directly connected to the submodules. The DC circulating current and the fundamental frequency circulating current were extracted and corrected to balance the power among the phases and the upper and lower bridge arms. This method is more complicated in the extraction process and requires an additional DC circulating current suppressor. Literature [19] introduced an MMC energy management system based on the EV battery, which adopted a two-level SOC equalization correction control strategy of phase unit and upper and lower bridge arms to achieve the SOC equalization of each energy storage submodule, but the upper and lower bridge arm equalization correction control of PR control was not considered. Due to the bandwidth limitation, the equalization correction control can only complete the zero-static-error tracking of signals with fixed frequency and cannot guarantee the accuracy of the energy equalization of the upper and lower bridge arms. In literature [20], under the condition of the unbalanced grid-side voltage, DC circulation injection is used to achieve the SOC equalization, but the SOC equalization of upper and lower bridge arms was not considered. Literature [21] used the three-level SOC equalization correction control to achieve the SOC equalization of each energy storage submodule under the unbalanced three-phase power grid, but the SOC equalization correction control layer of the upper and lower arms did not perform signal processing on the output correction. Harmonic signals of different frequencies caused fluctuations in the power difference between the upper and lower bridge arms. Literature [22] introduced that the energy storage battery was connected to the MMC submodule system through a Bi-directional DC-DC, and the SOC control was realized. In the upper and lower bridge arm balance control layer, only the three-phase SOC correction was averaged, and the accuracy of the correction was slightly deficient.

Based on the above, this paper proposes an improved three-level SOC equalization correction control strategy for the MMC-BESS based on analyzing the characteristics of the difference between the phase unit power and the bridge arm power. Feedforward is used in the SOC equalization correction control layer of upper and lower bridge arms. The sliding window integral method is used to process the harmonic signals of the correction value, so as to realize the accurate equalization of the power of the upper and lower arms of each phase unit, which can make the SOC of each energy storage submodule more quickly balanced and converged.

In Section 1, the operating state of the MMC-BESS, the main circuit topology, and the principle of the energy storage submodule are analyzed, and the voltage/current switching function model of phase unit bridge arm is established. Based on this, the internal characteristics of phase unit and bridge arm unit are analyzed. When not considering the capacitor voltage fluctuation of the submodule, the phase unit power is composed of the DC component, the double frequency AC component, and the AC output. The power difference between the upper and lower bridge arms is composed of the fundamental frequency component and the fundamental frequency AC output. If the capacitor voltage fluctuation of the submodule is considered, the phase unit power will increase the fundamental frequency circulating current component, and the power difference between the upper and lower bridge arms will increase the DC circulating current component. The results show that the AC fundamental frequency/double frequency circulation and DC circulation have an important influence on the average power distribution of the phase unit and the accurate power distribution of upper and lower bridge arms.

Section 2 constructs its double closed-loop control system based on the mathematical model of the MMC-BESS single-phase equivalent circuit and introduces the principle and stability analysis of the double closed-loop control system of the Bidirectional DC-DC converter applied to the energy storage submodule. A three-level SOC control system model is constructed based on interphase, upper and lower bridge arms, and each submodule. In the upper and lower bridge arm equalization control [23], the correction factor and the feedforward sliding window integral method are introduced [24, 25]. Compared with the traditional optimal one-third average method, which only distributes the DC circulation bias to three phases evenly, the feedforward sliding window integral method completely suppresses the DC circulation bias.

In Section 3, the lithium battery of energy storage submodule is continuously discharged, and the three-level SOC equalization correction controller is started under the conditions of sudden change of DC load/50% drop of two-phase voltage of the three-phase AC power grid. The results show that the DC bus voltage is stable at 20 kV under both working conditions. When the two-phase voltage drops, the three-phase AC current can be effectively compensated and balanced. Compared with the one-third average method, the three-level SOC equalization correction control strategy

proposed in this paper makes the capacitor voltage of the submodule stable at 5000 V under the condition of high current discharge, and the fluctuation rate and total harmonic distortion rate are smaller. The three-phase circulating current suppression effect of the system is better, so the phase unit power distribution is more balanced, and the upper and lower bridge arm power distribution is more accurate. Through comparative analysis, the SOC equalization correction control proposed in this paper makes the SOC of three-phase lithium battery have faster equalization convergence speed and better consistency.

2. Basic Principle of Energy Storage MMC

2.1. MMC-BESS Operating Status Analysis. The AC/DC grid system structure is shown in Figure 1. On the AC bus side, the MMC-BESS can be used as a power conversion and energy storage system for wind power generation units, and it can also be connected to a higher voltage grid. On the DC bus side, the MMC-BESS can complete DC energy interaction with photovoltaic power generation units, electric vehicles, energy feedback systems, etc. On the energy storage unit side, if the input/output power of the AC bus side and the DC bus side are equal, the MMC-BESS can be used as an AC/DC power converter. Therefore, the MMC-BESS can be equivalent to a three-port grid for power transmission among the AC bus side, the DC bus side, and the lithium battery energy storage system. There are 12 operating conditions in total. The working conditions simulated in this paper are DC load sudden change and two-phase voltage drop of three-phase network side voltage by 50%. The Bidirectional DC-DC converter of MMC-BESS energy storage system works in boost mode, and the lithium battery is continuously discharged.

2.2. MMC-BESS Topology. As shown in Figure 2, the MMC-BESS has the same three-phase structure and is connected in parallel to the DC bus side. Each phase can be divided into upper and lower bridge arms. Each bridge arm is composed of N energy storage submodules containing lithium batteries in series with the bridge arm inductor L_{em} and the bridge arm equivalent resistor R_{em}.

where u_{px} and u_{nx} represent the output voltage of the upper and lower bridge arm of energy storage submodules of phase X, respectively; i_{px} and i_{nx} represent the currents flowing through upper and lower bridge arms of phase X, respectively; e_x and i_x represent the x-phase voltage and current of the AC bus side, respectively. The number of phases $x = a, b,$ c. L_s is the balanced filter inductor between the AC bus and the AC output port of the MMC-BESS. U_{dc} represents the DC bus voltage.

2.2.1. Energy Storage Submodule. As shown in Figures 3 and 4, the energy storage submodule is composed of a half-bridge submodule and an energy storage system. By controlling the switching states of the half-bridge submodules VT_1 and VT_2, the charging and discharging of the capacitor C_{m} are changed to maintain the stability of the DC voltage of each phase. The energy storage system includes the Bidirectional DC-DC, energy storage filter inductor L_{bat} and the lithium battery. When the Bidirectional DC-DC converter operated in the Buck mode, the half-bridge submodule capacitor charged the lithium battery. The capacitor voltage of the half-bridge submodule was greater than its ideal value, VT_3 was turned on, and the half-bridge submodule discharged to the lithium battery. The capacitor voltage of half-bridge submodule was equal to or less than its ideal value, VD_4 was turned on, and there was no energy interaction between them. When the Bidirectional DC-DC operated in the Boost mode, the lithium battery charged the capacitor of the half-bridge submodule. The capacitor voltage of the half-bridge submodule was less than its ideal value, VD_3 was turned on, and the lithium battery charged the capacitor of the half-bridge submodule. The capacitor voltage of the half-bridge submodule was equal to or greater than its ideal value, VT_4 was turned on, and there was no energy interaction between them. From the above Bidirectional DC-DC working mode analysis, it can be seen that the lithium battery of the energy storage system operated in a low-voltage condition, and the charging and discharging current had a high degree of controllability (Table 1).

2.2.2. Bridge Arm Voltage/Current Switching Function Model. During the stable operation of the MMC-BESS, the capacitor of the energy storage submodule not only flows through the bridge arm current for energy interaction with AC and DC sides, but also flows the charging and discharging current of the lithium battery in the energy storage system. Taking one phase as an example, the switching function s of its energy storage submodule is defined as

$$s = \begin{cases} 1, & \mathrm{VT}_1\,(\mathrm{on}), \mathrm{VT}_2\,(\mathrm{off}), \\ 0, & \mathrm{VT}_1\,(\mathrm{off}), \mathrm{VT}_2\,(\mathrm{on}). \end{cases} \tag{1}$$

Thus, the output voltage of the energy storage submodule port of phase unit bridge arm is expressed as

$$\begin{cases} u_{ixk} = s_{ixk} U_{smk}, \\ C_m \dfrac{\mathrm{d}U_{\mathrm{smk}}}{\mathrm{d}t} = s_{ixk} i_{ix} + i_{Lbk}, \end{cases} \tag{2}$$

where u_{ixk} is the output voltage value of the k-th submodule in the upper or lower bridge arm of one phase, U_{smk} is the capacitor voltage of the submodule, and s_{ixk} is the switching function; i_{ix} is the current of the upper or lower bridge arm of one phase, and i_{Lbk} is charging and discharging current of the lithium battery of the energy storage system. In equation (2), $i = p$ (upper bridge arm) or n (lower bridge arm), the number of phases $x = a, b,$ c; $k = 1 \sim N$ representing the number of submodules of the same bridge arm.

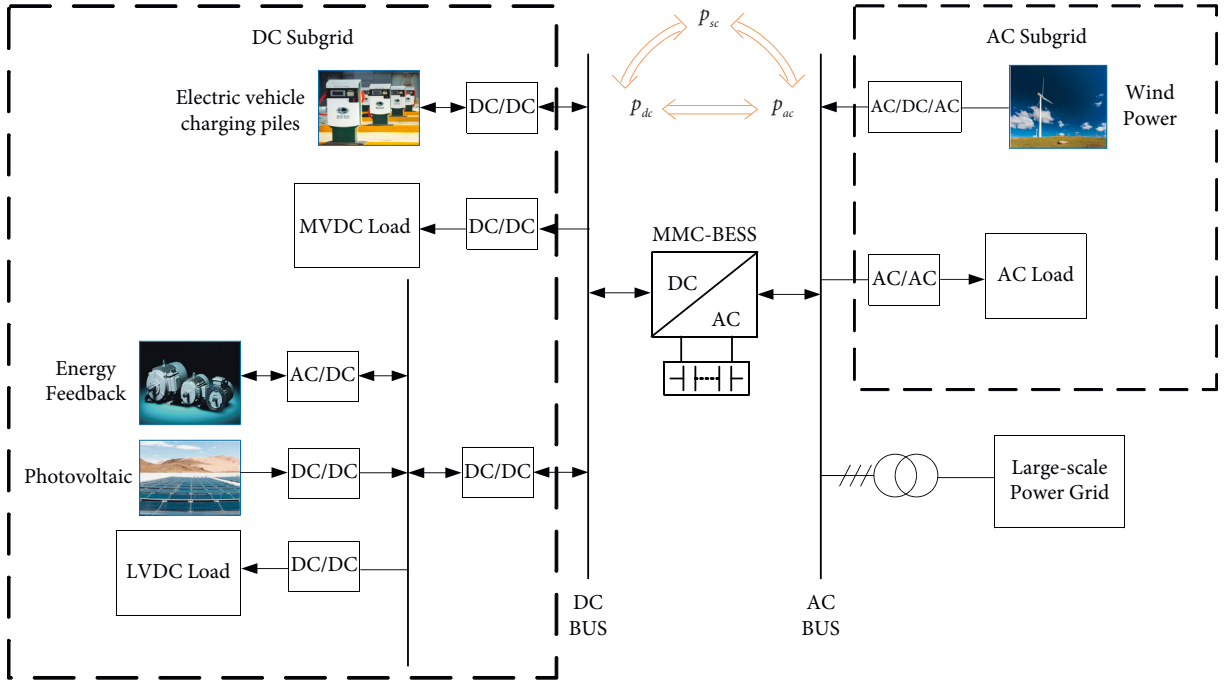

Figure 1: AC/DC grid system structure.

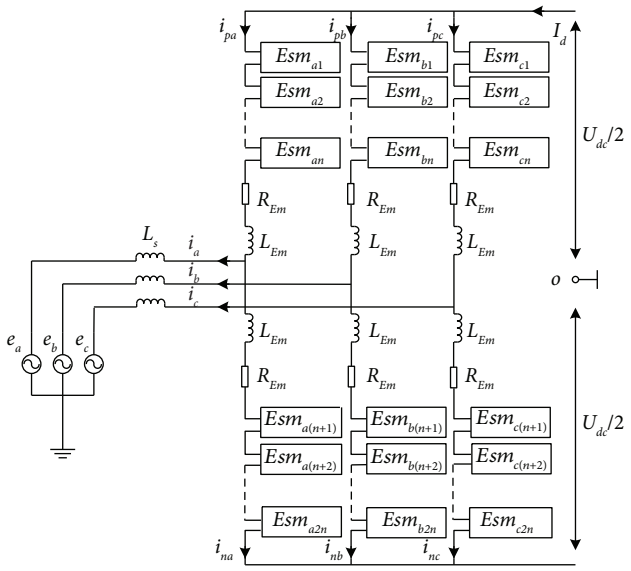

Figure 2: MMC-BESS main circuit topology.

Therefore, the bridge arm output voltage u_{ix} and output current i_{ix} can be expressed as

$$\begin{cases} u_{ix} = \sum_{k=1}^{N} s_{ixk} U_{smk}, C_m \dfrac{d\sum_{k=1}^{N} s_{ixk} U_{smk}}{dt} = i_{ix} + \sum_{k=1}^{N} s_{isk} i_{Lbk}. \end{cases} \tag{3}$$

Ignoring the equivalent impedance of the bridge arm, the KVL equation for the upper and lower bridge arms is expressed as follows:

$$\begin{cases} u_{px} = \dfrac{1}{2} U_{dc} - E_a \sin(\omega t), \\ u_{nx} = \dfrac{1}{2} U_{dc} + E_a \sin(\omega t), \end{cases} \tag{4}$$

where u_{px} and u_{nx} are the upper and lower arm voltages of the x-th phase, respectively; E_a is the peak value of the AC voltage; U_{dc} is DC-side voltage.

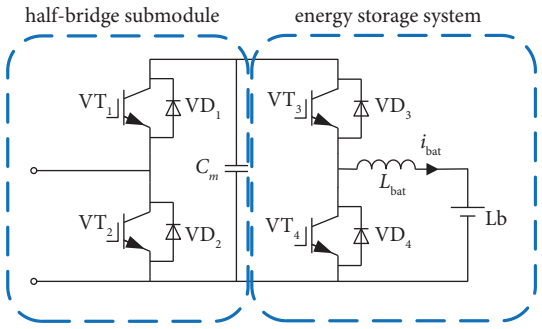

Figure 3: Energy storage submodule.

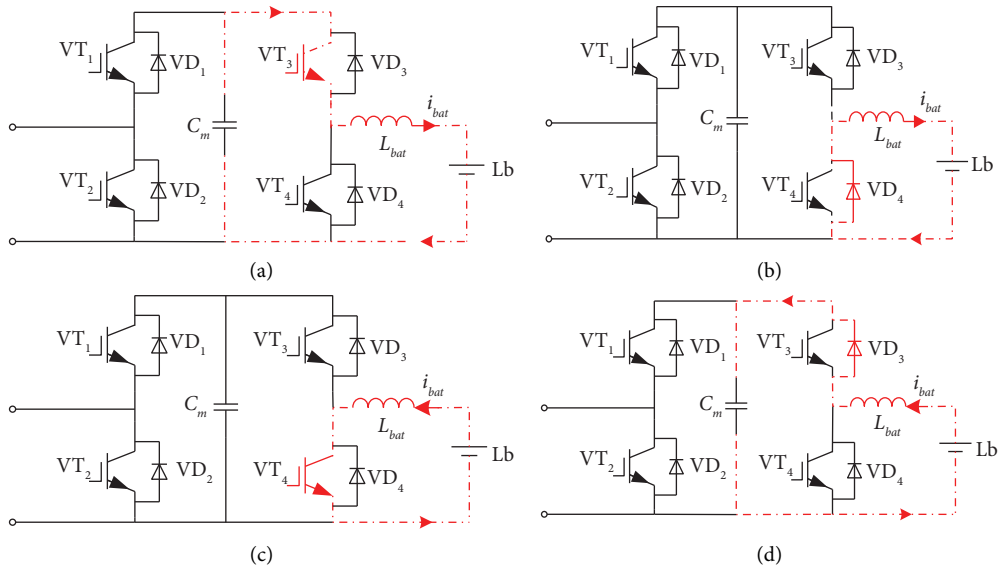

Figure 4: Energy interaction status of the lithium battery in the buck and boost working modes. (a) In the buck mode, with energy interaction. (b) In the buck mode, without energy interaction. (c) In the boost mode, without energy interaction. (d) In the boost mode, with energy interaction.

2.2.3. Analysis of Internal Characteristics of Phase Unit and Bridge Arm Unit. In order to achieve a better control effect and master the control law of the MMC-BESS, the internal characteristics of the phase unit and the bridge arm unit are analyzed. According to equations (4), the following equations are obtained:

$$\begin{cases} u_{px} = \dfrac{\sum_{k=1}^{N} U_{\text{smk}}}{2} - \dfrac{\sum_{k=1}^{N} mU_{\text{smk}} \sin(\omega t)}{2}, \\ u_{nx} = \dfrac{\sum_{k=1}^{N} U_{\text{smk}}}{2} + \dfrac{\sum_{k=1}^{N} mU_{\text{smk}} \sin(\omega t)}{2}, \end{cases} \tag{5}$$

where m is the modulation ratio, and U_{smk} is the capacitor voltage of the energy storage submodule, which is put into operation in the x-th phase. Based on the single-phase equivalent circuit, the KAL equation of the upper and lower bridge arms is obtained as follows:

$$\begin{cases} i_{px} = \dfrac{1}{3} I_{dc} + \dfrac{I_x \sin(\omega t - \varphi)}{2}, \\ i_{nx} = \dfrac{1}{3} I_{dc} - \dfrac{I_x \sin(\omega t - \varphi)}{2}, \end{cases} \tag{6}$$

where i_{px} and i_{nx} are the currents flowing through the upper and lower bridge arms, I_{dc} is the DC output current, I_x is the peak value of the phase AC current, and φ is the impedance angle. From (5) and (6), the power of phase unit and upper and lower bridge arms can be obtained expressed as (7) and (8) (without considering the capacitor voltage of the submodule):

Table 1: MMC-BESS interaction status and energy storage system working mode.

MMC-BESS interaction status	DC-DC working mode	Lithium battery charge/discharge status	VT_3	VT_4	Submodule capacitor voltage status	Circuit
$p_{bat} = 1$ (absorbed power)	Buck mode	Charge	PWM	0	$U_{sm} > U_{smref}$ $U_{sm} < U_{smref}$	Figure 4(a) Figure 4(b)
$p_{bat} = 1$ (output power)	Boost mode	Discharge	0	PWM	$U_{sm} > U_{smref}$ $U_{sm} < U_{smref}$	Figure 4(c) Figure 4(d)

Note. U_{sm} represents the actual value of the submodule capacitor voltage; U_{smref} represents the ideal value of the submodule capacitor voltage.

$$p_x = \underbrace{\frac{I_{dc}\sum_{k=1}^{N} U_{smk}}{3}}_{\text{DC component}} + \underbrace{\frac{I_x\sum_{k=1}^{N} mU_{smk}\cos 2\omega t}{4}}_{\text{double frequency AC component}} - \underbrace{\frac{I_x\sum_{k=1}^{N} mU_{smk}\cos\varphi}{4}}_{\text{AC output}}, \tag{7}$$

$$\Delta p_x = \underbrace{\frac{I_{dc}\sum_{k=1}^{N} mU_{smk}\sin\omega t}{3} + \frac{I_x\sum_{k=1}^{N} U_{smk}\cos\omega t\sin\varphi}{2}}_{\text{fundamental frequency AC component}} - \underbrace{\frac{I_x\sum_{k=1}^{N} U_{smk}\sin\omega t\cos\varphi}{2}}_{\text{AC output}}, \tag{8}$$

where p_x represents the power of the phase unit, and Δp_x represents the power difference of upper and lower bridge arms.

When considering capacitor voltage fluctuation of the submodule, p_x and Δp_x are, respectively, expressed as (9) and (10):

$$p_x = \underbrace{\frac{I_{dc}\sum_{k=1}^{N} U_{smk}}{3}}_{\text{DC component}} + \underbrace{\frac{I_x\sum_{k=1}^{N} mU_{smk}\cos 2\omega t}{4}}_{\text{double frequency AC component}} - \underbrace{\frac{I_x\sum_{k=1}^{N} mU_{smk}\cos\varphi}{4}}_{\text{AC output}} + \underbrace{\left|\frac{I_{dc}\sum_{k=1}^{N} m\Delta U_{smk}\sin\omega t}{6}\right|}_{\text{Fundamental frequency AC circulating current component}}, \tag{9}$$

$$\Delta p_x = \underbrace{\frac{I_{dc}\sum_{k=1}^{N} mU_{smk}\sin\omega t}{3} + \frac{I_x\sum_{k=1}^{N} U_{smk}\cos\omega t\sin\varphi}{2}}_{\text{fundamental frequency AC component}} - \underbrace{\frac{I_x\sum_{k=1}^{N} U_{smk}\sin\omega t\cos\varphi}{2}}_{\text{AC output}} + \underbrace{\left|\frac{I_{dc}\sum_{k=1}^{N} \Delta U_{smk}}{6}\right|}_{\text{DC circulating current component}}. \tag{10}$$

By comparing (7) with (9), it can be seen that when considering the fluctuation of the capacitor voltage of the submodule, the phase unit power will increase the fundamental frequency AC circulating current component. By comparing (8) with (10), it can be seen that when considering the fluctuation of the capacitor voltage of the submodule, the power difference between upper and lower bridge arms will increase the DC circulating current component. Figures 5 and 6 are the power difference curves between the phase unit and the upper and lower bridge arms, which are drawn according to the actual parameters of the system. In Figure 5, the green curve includes the DC component and AC output. The blue curve includes the DC component, the double frequency AC component, and AC output. The red curve includes DC component, the double frequency AC component, the fundamental frequency circulation component, and AC output. It shows that the fundamental frequency circulating current component formed by the capacitor voltage fluctuation of the submodule caused uneven power distribution of the phase unit.

In Figure 6, the blue curve includes the AC component, the fundamental frequency, and AC output. The red curve includes the fundamental frequency AC component, AC output, and the DC circulation component. It shows that the DC circulating current caused by the capacitor voltage fluctuation of the submodule caused the inaccurate power distribution of the upper and lower bridge arms.

Therefore, the essential reason for constructing the three-level SOC equalization correction control is to suppress the fundamental frequency circulation of phase unit and the DC circulation of upper and lower bridge arms caused by the fluctuation of capacitor voltage of submodule.

3. MMC-BESS Hierarchical Control System

The MMC-BESS hierarchical control is shown in Figure 7, which is mainly composed of the main control system, the three-level SOC equalization correction control, and the Bidirectional DC-DC converter control system based on PI control. The main control system collected the active and

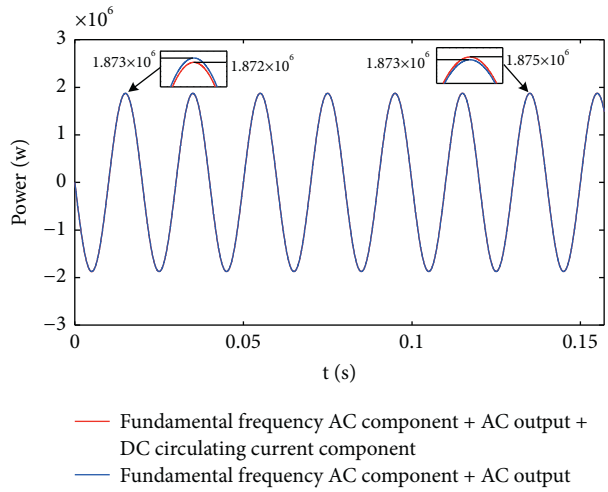

Figure 5: Phase unit power.

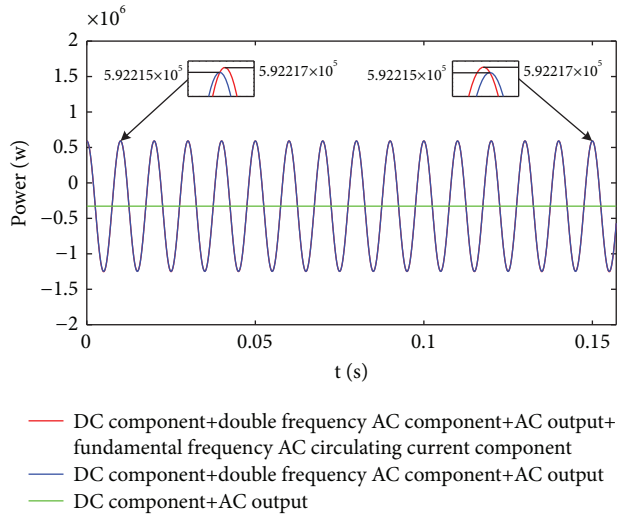

Figure 6: Power difference between upper and lower bridge arms.

reactive power of the main circuit of the MMC, adjusted it by the PI controller, and generated the three-phase sinusoidal modulation wave after feedforward decoupling. The generated three-phase sinusoidal modulation wave was sent to the carrier phase-shifting modulation through the correction of the three-level SOC equalization control and worked with the submodule capacitor voltage quicksort algorithm to generate the triggering pulse of the power switch of each half-bridge submodule of the MMC-BESS main circuit. The Bidirectional DC-DC converter adopted the double closed-loop control system structure of the outer loop voltage and inner loop current based on the PI controller to realize the energy interaction between the MMC and the lithium battery of the energy storage submodule.

3.1. MMC-BESS Main Control System

3.1.1. MMC-BESS Mathematical Model of Single-Phase Equivalent Circuit. Based on the analysis of the internal characteristics of the phase unit and the bridge arm unit, in order to achieve effective control and interaction of the AC and DC-side energy, the MMC-BESS phase unit was used as a "bridge" to establish the AC and DC-side voltage/current relationship. The single-phase equivalent circuit is shown in

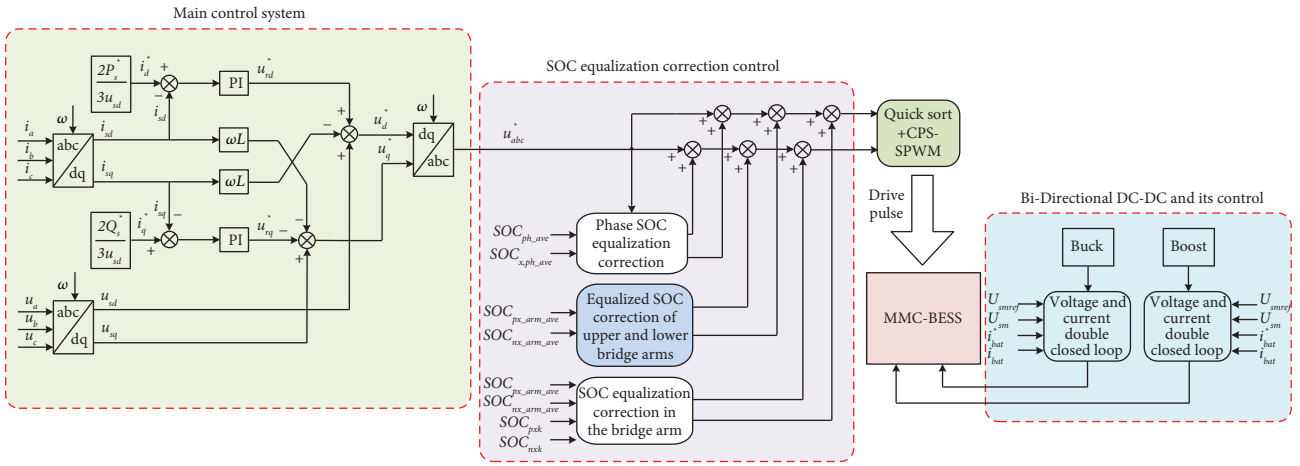

Figure 7: MMC-BESS hierarchical control system.

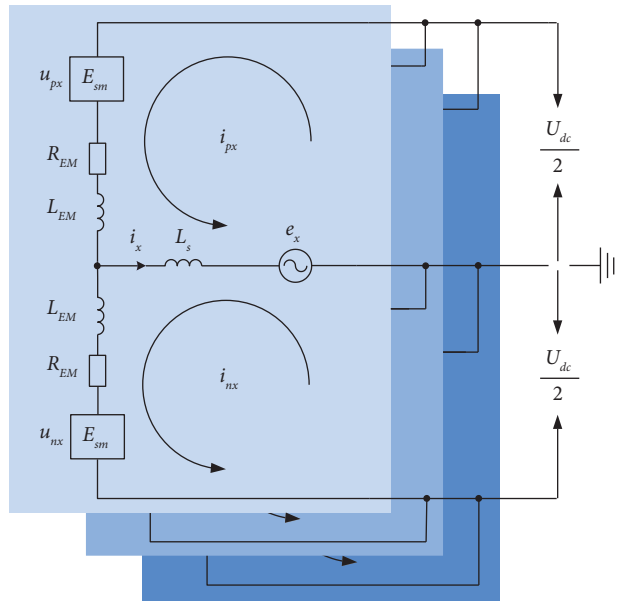

Figure 8: MMC-BESS single-phase equivalent circuit model.

Figure 8, taking phase A as an example for description. The expressions are as follows:

$$\begin{cases} L_{Em}\dfrac{\mathrm{d}i_{pa}}{\mathrm{d}t} + R_{Em}i_{pa} + L_s\dfrac{\mathrm{d}i_a}{\mathrm{d}t} = \dfrac{U_{\mathrm{dc}}}{2} - e_a - u_{pa}, \\ L_{Em}\dfrac{\mathrm{d}i_{na}}{\mathrm{d}t} + R_{Em}i_{na} - L_s\dfrac{\mathrm{d}i_a}{\mathrm{d}t} = \dfrac{U_{\mathrm{dc}}}{2} + e_a - u_{na}, \end{cases} \tag{11}$$

$$\begin{cases} i_{pa} = \dfrac{I_{dc}}{3} + \dfrac{i_a}{2}, \\ i_{na} = \dfrac{I_{dc}}{3} - \dfrac{i_a}{2}. \end{cases} \tag{12}$$

From equations (11), the following equation can be obtained:

$$\left(L_s + \frac{L_{Em}}{2}\right)\frac{\mathrm{d}i_a}{\mathrm{d}t} + \frac{R_{Em}}{2}i_a = \frac{u_{na} - u_{pa}}{2} - e_a. \tag{13}$$

According to (13), the AC-side current can be changed by controlling the bridge arm voltage difference.

In order to facilitate the design of the control system, (13) can be extended to the three-phase expression, which can be transformed by $abc/\mathrm{d}q$ transformation matrix $M(\theta)_{abc\text{-}\mathrm{d}q}$ from the three-phase static coordinate system to the two-phase rotating coordinate system. Thus, the following equations can be obtained:

$$\begin{cases} P_s^* = \dfrac{3}{2}Ei_d^*, \\ \\ Q_s^* = -\dfrac{3}{2}Ei_q^*. \end{cases} \tag{14}$$

3.1.2. Structure and Principle of Main Control System. The main control system of the MMC-BESS is shown in Figure 9. Firstly, according to the instantaneous active/reactive power theory, the active/reactive power reference values P_S^* and Q_S^* are transformed to obtain the current reference values of axes d and q, namely, i_d^* and i_q^*.

Secondly, the three-phase AC currents i_a, i_b and i_c are transformed by abc/dq coordinates to realize the separation of active and reactive power, and then, i_{sd} and i_{sq} are obtained. The reference value voltages u_{rd}^* and u_{rq}^* of axes d and q are obtained after making the difference with the actual value based on the PI control. According to (14), in order to accelerate the operation of the system and remove the voltage/current coupling on AC side of axes d and q, a feedforward decoupling is added. The three-phase AC voltages u_a, u_b and u_c were transformed by $abc/\mathrm{d}q$ coordinates to obtain u_{sd} and u_{sq}, which were combined with coupling currents of u_{rd}^* and u_{rq}^* of axes d and q to complete the feedforward decoupling to obtain the ideal voltage value of u_d^* and u_q^* of axes d and q. Finally, the three-phase AC voltage modulation waveform was obtained through $\mathrm{d}q/abc$ inverse coordinate transformation.

3.2. The Bidirectional DC-DC Converter and Its Control. The energy storage system consists of the energy storage battery and the Bidirectional DC-DC converter. The Bidirectional DC-DC converter adopted PI-based double closed-loop control of outer loop voltage/inner loop current. The actual value of the inner loop current was the inductor current of the Bidirectional DC-DC converter, which was controlled to stabilize the power balance of each energy storage submodule. The actual value of the outer loop voltage was the capacitor voltage of the energy storage submodule, which was controlled to stabilize the capacitor voltage of the submodule.

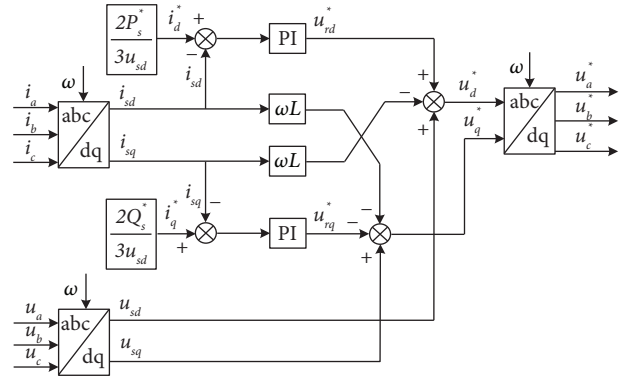

Figure 9: MMC-BESS main control system.

The structure of the Bidirectional DC-DC converter control system is shown in Figure 10. The difference between the reference value U_{smref} and the actual value U_{sm} of each phase of the energy storage submodule capacitor voltage is obtained after PI tracking control, thus obtaining the reference value of the inductor current of the energy storage system. Then, the difference is made with the actual value i_{bat}. The loop PI is adjusted and compared with the carrier to generate the PWM pulse signals. The switching between the Buck and the Boost mode needs to set conditions. In the control system, when the reference value of inductor current is multiplied by −1, the Bidirectional DC-DC works in the Boost mode.

Taking Boost as an example, the stability analysis of the control system is carried out, and the constructed double closed-loop transfer function is

$$G(s) = \frac{G_{PI_1}(s).G_{PI_2}(s)}{1 + G_{PI_1}(s)\cdot G_{PI_2}(s) + G_{PI_2}(s)\cdot C_m s + L_{\mathrm{bat}}C_m s^2}. \tag{15}$$

The transfer function structure and the system Bode diagram of the double closed-loop control system of the outer loop voltage and inner loop current based on PI control are shown in Figures 11 and 12, respectively.

In the transfer function, P_1, P_2 and P_3 are the forward channel loop composed of the half-bridge submodule capacitor voltage U_{sm}, the filter inductor current of energy storage system i_{bat} and the difference between the lithium battery voltage U_{bat} and U_{sm}. The specific expressions are as follows:

$$\begin{cases} P_1 = -G_{PI_1}(s)\cdot G_{PI_2}(s)\cdot \dfrac{1}{L_{\mathrm{bat}}C_m s^2}, \\ \\ P_2 = -G_{PI_2}(s)\cdot \dfrac{1}{L_{\mathrm{bat}}s}, \\ \\ P_3 = -\dfrac{1}{L_{\mathrm{bat}}C_m s^2}. \end{cases} \tag{16}$$

In (15) and (16) and Figure 11, the expressions of $G_{PI_1}(s)$ and $G_{PI_2}(s)$ in frequency domain are $k_{p1} + k_{i1}/s$ and $k_{p2} + k_{i2}/s$. In this paper, $k_{p1} = 10$, $k_{i1} = 0.5$, $k_{p2} = 5$ and

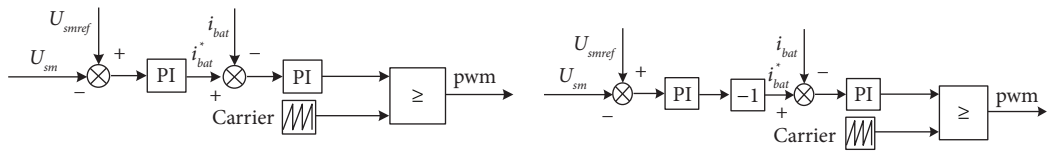

Figure 10: Bidirectional DC-DC control system.

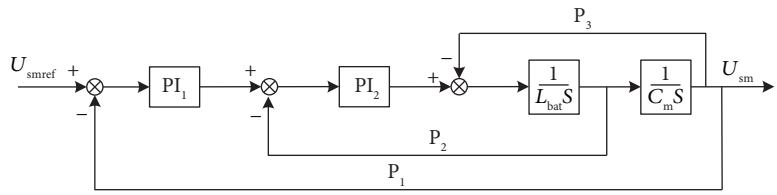

Figure 11: Transfer function structure of the bidirectional DC-DC double closed-loop control system.

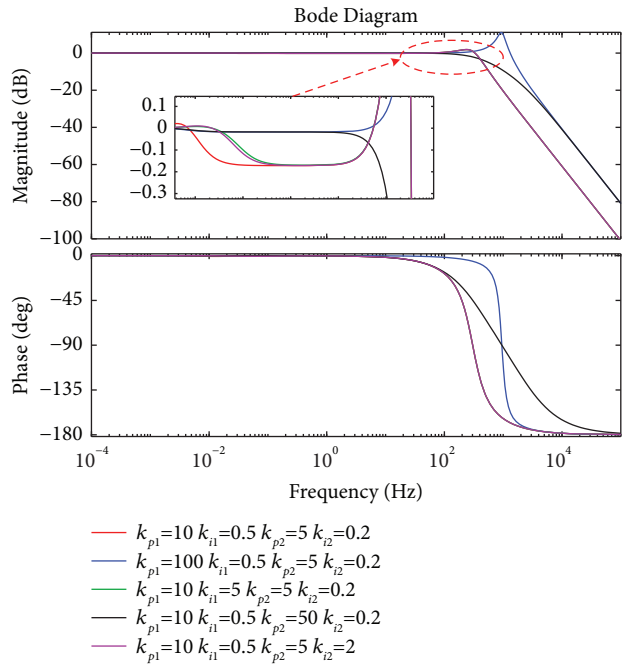

Figure 12: Comparison of amplitude phase frequency characteristics of bidirectional DC-DC double closed-loop control system.

$k_{i2} = 0.2$ are taken as basic variables. One variable is changed and expanded by 10 times each time, and the other three variables remain unchanged. A group of system Bode diagram curves are drawn, as shown in Figure 12. After analysis and comparison, $k_{p1} = 100$, $k_{i1} = 0.5$, $k_{p2} = 5$ and $k_{i2} = 0.2$ are finally selected. The resonant peak frequency of the double closed-loop control system constructed by this group of variables is about 3184 Hz, and the switching frequency of the Bidirectional DC-DC converter in this paper is 10 kHz. It shows that the switching frequency signal greater than the resonant peak frequency is well suppressed under the high current and rapid charge and discharge condition of the lithium battery in the energy storage system, and the capacitor voltage signal of the submodule less than the resonant peak frequency will complete the zero static error tracking of its ideal input value after passing through the control system.

3.3. SOC Equalization Correction Control. The essence of the SOC equalization correction control of the MMC-BESS is to perform power correction on the three phases, upper and lower bridge arms, and their submodules, respectively. Firstly, through the analysis of the three-level SOC equalization control process, the feedforward sliding window integral method was introduced into the upper and lower bridge arm control layer to form a more accurate equalization correction, so as to make full use of the lithium battery capacity of the energy storage submodule.

3.3.1. Phase-To-Phase SOC Equalization Correction Control. In order to effectively correct the DC current components in the three-phase MMC-BESS, during the SOC balance correction control of the phase unit, the PI adjustment method is used to realize the zero-static-error tracking of the average

SOC of each-phase submodule to the average SOC of the three-phase submodule.

The specific phase equalization control structure is shown in Figure 13. The average SOC of lithium battery of each energy storage submodule in phase X is $\mathrm{SOC}_{x,\ \mathrm{ph\_ave}}$, and the average SOC of lithium battery of the three-phase energy storage submodule is $\mathrm{SOC}_{\mathrm{ph\_ave}}$. The mathematical expression is as follows:

$$\begin{cases} \mathrm{SOC}_{x,ph\_\mathrm{ave}} = \dfrac{\sum_{k=1}^{2N} \mathrm{SOC}_{x,k}}{2N}, \\ \mathrm{SOC}_{ph\_\mathrm{ave}} = \\ \dfrac{\mathrm{SOC}_{a,ph\_\mathrm{ave}} + \mathrm{SOC}_{b,ph\_\mathrm{ave}} + \mathrm{SOC}_{c,ph\_\mathrm{ave}}}{3}. \end{cases} \tag{17}$$

3.3.2. SOC Equalization Correction Control of Upper and Lower Bridge Arms Based on Feedforward Sliding Window Integral

$$\begin{cases} \mathrm{SOC}_{px\_\mathrm{arm\_ave}} = \dfrac{\sum_{k=1}^{N} \mathrm{SOC}_{pxk}}{N}, \\ \mathrm{SOC}_{nx\_\mathrm{arm\_ave}} = \dfrac{\sum_{k=1}^{N} \mathrm{SOC}_{nxk}}{N}. \end{cases} \tag{18}$$

It can be seen from formula (18) that the DC circulating current has the same effect on the power of the upper and lower bridge arms, and the power flow can be adjusted among the three phases. In order to obtain more accurate power distribution of the power of the upper and lower bridge arms, the upper and lower bridge arm correction factor h_{cps_x} and the feedforward sliding window integral are introduced. As shown in Figure 14, the correction factor h_{cps_x} contains the DC component, the fundamental frequency AC component, and other frequency AC components, which are multiplied by e_{aref} and go through the sliding window integral to obtain the equalization correction of the upper and lower bridge arms $U^{*}_{\mathrm{arm\_cps}}$ containing only the fundamental frequency and a small amount of AC component of other frequencies. The filtering integral process is as follows:

$$\int_{t}^{t+T} \sin(\omega t) \cdot \left[A\sin(\omega t) + \sum_{k'=2}^{\infty} B_{k'} \cdot \sin\left(k'\omega t + \varphi_{k'}\right) \right] dt. \tag{19}$$

Both T in (19) and Z^{-N} in Figure 14 represent the delay, with the delay time being 0.2 s, and the minimum filtering frequency is 5 Hz.

3.3.3. SOC Equalization Correction Control in Bridge Arms. The SOC equalization correction control of the lithium battery of each submodule in the bridge arms is the same as the interphase SOC equalization correction control. Making the difference between the average value of the SOC of the lithium battery of the upper and lower bridge arm energy storage submodule and the actual value of the lithium battery of each submodule, the zero-static-error tracking of both through the PI controller was realized. When the MMC-BESS is in discharging condition, the Bidirectional DC-DC worked in the Boost mode. If the SOC value of the lithium battery was large, the discharging current would increase; if the SOC value was small, the discharging current would decrease. Under charging conditions, the Bidirectional DC-DC is switched to the Buck mode, and if the SOC value of the lithium battery was small, the charging current would increase; if the SOC was large, the charging current would be reduced.

Eventually, the working state modulation commands of each submodule of the MMC-SCESS were modified and acted on each of the three-phase bridge arms and their submodules, respectively, so that the phase-to-phase power and the power of upper and lower bridge arms was corrected, and then it was combined with the quicksort algorithm of the submodule capacitor voltage, thus quickly balancing the capacitor voltage of each phase submodule. Based on this, the double frequency circulating current among phases was suppressed, and the system loss was reduced, as shown in Figure 15.

4. Simulation

In order to verify the effectiveness of the proposed three-level SOC equalization correction control strategy based on the feedforward sliding window integral method, a three-phase five-level MMC-BESS model was constructed in the Matlab/Simulink environment. The parameters are shown in Table 2. Due to the limitation of the computer system performance, the number of submodules of the upper and lower bridge arms was set to 4 in the simulation verification. In practical applications, due to the scalability of the MMC-BESS, more input submodules could jointly withstand the DC voltage of 20 kV on the DC side of each phase unit. This paper focuses on the following three aspects under the discharging state of lithium battery energy storage system: (1) the sudden change of DC-side load, aiming at stabilizing the DC bus voltage; (2) the two-phase drop of the three-phase grid-side voltage and the three-phase current balance compensation capability; (3) a faster equalization convergence speed of the SOC of each phase of the proposed three-level SOC equalization correction control strategy under the above two working conditions.

As shown in Figures 16–18, in the first working condition, the DC load increased suddenly at 0.5 s after the system was started. In order to quickly stabilize the DC bus voltage and maintain power balance, the MMC-BESS input the lithium battery and the three-level SOC balance correction controller. The Bidirectional DC-DC of the MMC-BESS energy storage system worked in the Boost mode, and the lithium battery continued to discharge. When the load changed suddenly, the DC voltage was 19800 V and finally stabilized at 20 kV. In the second working condition, after the first working condition lasted for 0.5 s, at 1 s, the DC load recovered, the three-phase grid-side voltages B and C

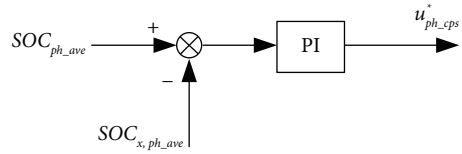

Figure 13: Phase-to-phase SOC equalization correction control.

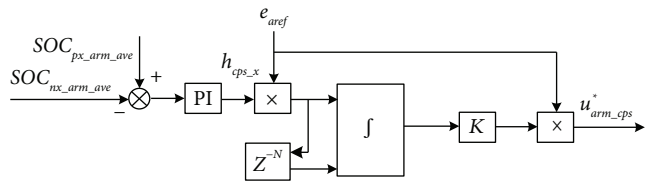

Figure 14: Equalization correction control of upper and lower bridge arms.

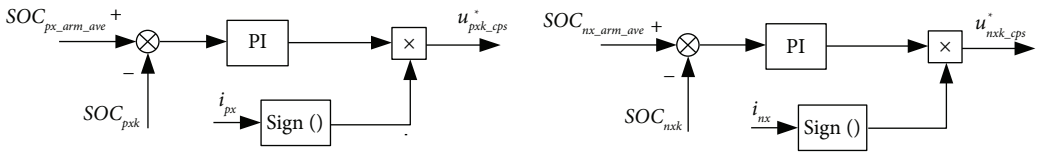

Figure 15: SOC equalization correction control of submodules in bridge arms.

Table 2: System simulation parameters.

Parameters	Value
The number of bridge arm submodules of each phase n	4
Rated capacity S/MVA	5
Grid phase voltage E_j/kV	5.7
DC-side voltage U_{dc}/kV	20
Bridge arm filter inductor L_{Em}/mH	2
Submodule capacitor C_m/mF	4.7
Grid-side filter inductor L_S/mH	4
DC/DC inductor L_{bat}/mH	3
Switching frequency f/Hz	1000

dropped by 50%, and the peak phase voltage changed from 8000 V to 4000 V. The Bidirectional DC-DC of the MMC-BESS energy storage system still worked in the Boost mode, and the lithium battery continued to discharge to compensate for the difference of the three-phase power, so that the three-phase grid-side current increased and balanced. The DC bus voltage was stable at about 20 kV, the maximum variable was 1500 V, and the steady-state error was 7.5%. The maximum peak value of the three-phase current was 231.9 A, the effective value of the three-phase average current was 160.96 A, and the unbalance degree was 0.024. The parameters are shown in Table 3. The total harmonic distortion rate of the three-phase current is shown in Figure 19. Five power frequency cycles after 5.66 s were selected for measurement, and the total harmonic distortion rate was 1.38%.

The MMC-BESS acted as a bridge for energy conversion between the AC side, the DC side, and the energy storage battery. The stability of the capacitor voltage of submodule of each phase could prove the stability of the power input and output during the energy conversion period. The stability of the submodule capacitor voltage could not only reduce the double frequency circulation formed by the pressure difference between the phases of the MMC-BESS, but also reduce the circulating current in the upper and lower bridge arms formed by the fluctuation of the submodule capacitor voltage in the bridge arms of each phase.

Under the same operating condition, when the three-phase grid-side voltage dropped by 50%, the maximum capacitor voltage of the submodule of the c-phase upper and lower bridge arm before the improvement by using the one-third average method was 5009 V, and the minimum was 4991 V. The maximum capacitor voltage of the submodule of the improved c-phase upper bridge arm was 5008 V, and the minimum was 4992 V. In the range of 0.5 s to 9 s, the SOC equalization correction control strategy proposed in this paper and the three-stage SOC equalization correction control strategy using one-third average method were compared and analyzed with the total harmonic distortion rate of capacitor voltage of each submodule of phase C with 50 Hz as the fundamental frequency. It could be seen from the comparative analysis of Figure 20 and Table 4 that the total harmonic distortion rate of capacitor voltage of the submodule of c-phase lower bridge arm with the two methods is less than that of the upper bridge arm. For the same submodule, the total harmonic distortion rate of the capacitor voltage of the submodule using the method proposed in this paper is less than that of the same submodule using the one-third average method. It indirectly proved that the MMC-BESS using the SOC equalization correction control strategy proposed in this paper has more average phase-to-phase power distribution and more accurate power distribution of upper and lower bridge arms.

It can be seen from (10) and (11) that when the capacitor voltage fluctuation and total harmonic distortion rate of the submodule were smaller, the difference between the phase-

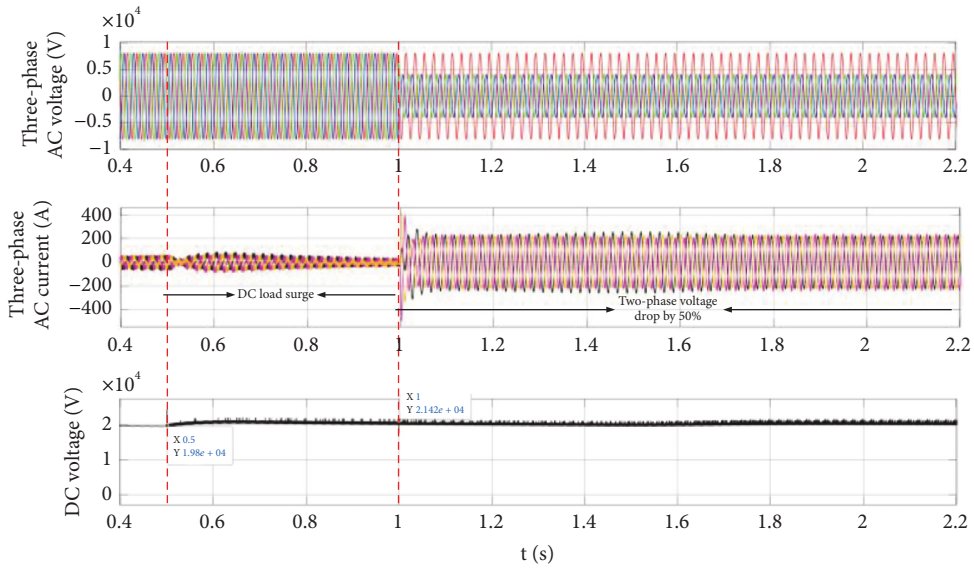

Figure 16: System three-phase voltage/current and DC voltage at 0.4 ~ 2.2 s.

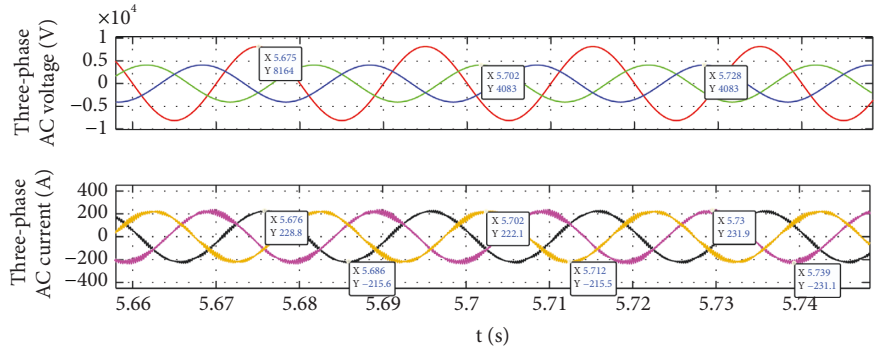

Figure 17: Three-phase AC voltage and current at 5.66 s ~ 5.76 s.

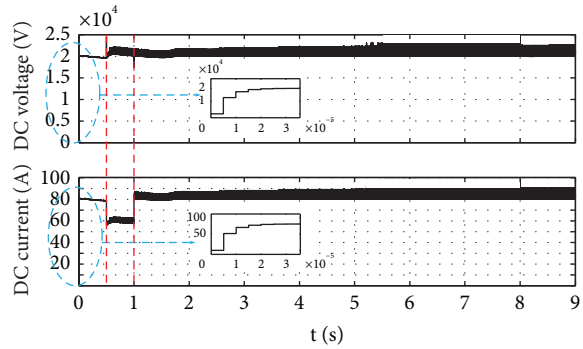

Figure 18: DC-side voltage and current at 0 ~ 9 s.

to-phase power of the system and the power of the upper and lower bridge arms of each phase should be smaller, so the three-phase circulating current should also be smaller. The reduction of the three-phase circulating current of the system was helpful in improving the efficiency of the MMC-BESS. Figure 21 shows the three-phase circulating current of the system using the two methods. The results showed that after the system was stable, under the working conditions with the load sudden change and two-phase voltage drop, the two methods could effectively suppress the three-phase circulating current, but the effect of using feedforward sliding window integral method on circulating current suppression was more obvious, and the peak value of circulating current was smaller. The maximum peak values of

Table 3: Unbalance degree parameters of three phases.

Phases x	Current peak of three phases (A)	Current effective value of three phases (A)	Average value of effective value of three-phase current (A)	Differential phase current (effective value of phase current - average value of effective value of three-phase current) (A)	Three-phase current unbalance degree (max effective value of differential phase current divided by average value of effective value of three-phase current)
A-phase	228.8	161.81	160.96	0.85	2.4%
B-phase	222.1	157.07		3.89	
C-phase	231.9	164.00		3.04	

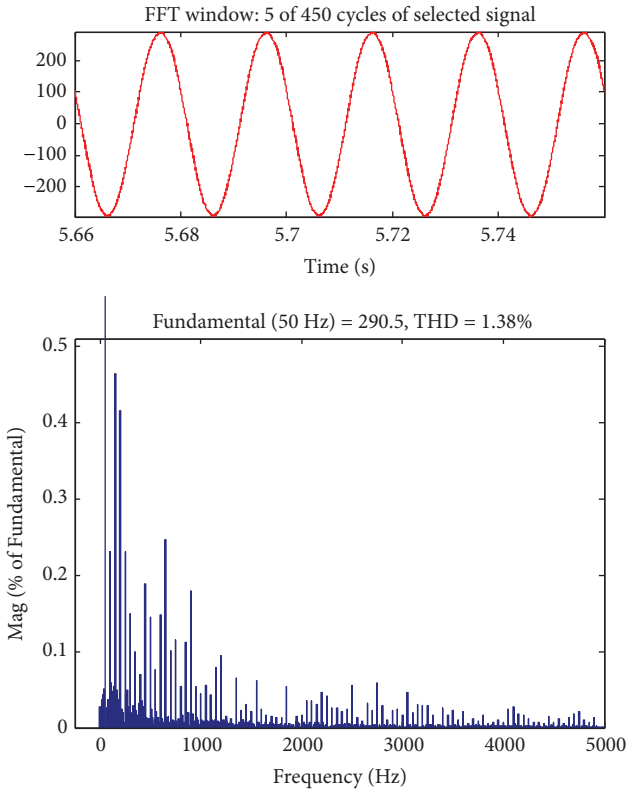

Figure 19: Three-phase grid-side current THD at 5 s.

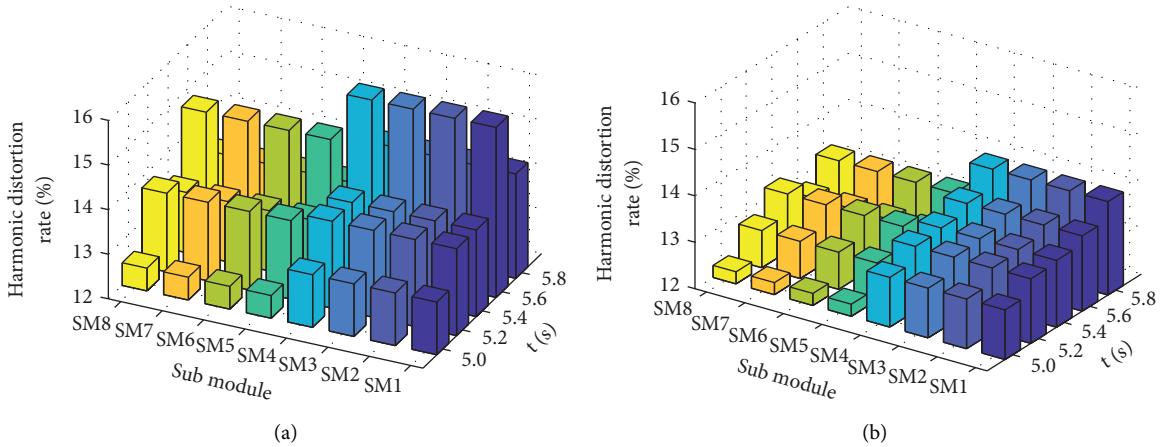

Figure 20: Analysis of harmonic distortion rate of capacitor voltage of c-phase submodule. (a) Harmonic distortion rate of each submodule using one-third average method. (b) Harmonic distortion rate of each submodule of sliding window integral method.

Table 4: Capacitor voltage distortion rate of *c*-phase submodule using one-third average method and sliding window integral method.

Harmonic distortion rate of capacitor voltage of submodule					
One-third average method:					
	5 s	5.2 s	5.4 s	5.6 s	5.8 s
Upper bridge arm of phase *C* (sm1 ~ sm4)	13.18%	13.95%	13.94%	15.81%	14.34%
Lower bridge arm of phase *C* (sm5 ~ sm8)	12.51%	13.76%	13.35%	14.72%	13.34%
Sliding window integral method:					
	5 s	5.2 s	5.4 s	5.6 s	5.8 s
Upper bridge arm of phase *C* (sm1 ~ sm4)	13.07%	13.39%	13.49%	13.62%	14.01%
Lower bridge arm of phase *C* (sm5 ~ sm8)	12.26%	12.80%	13.24%	12.81%	13.26%

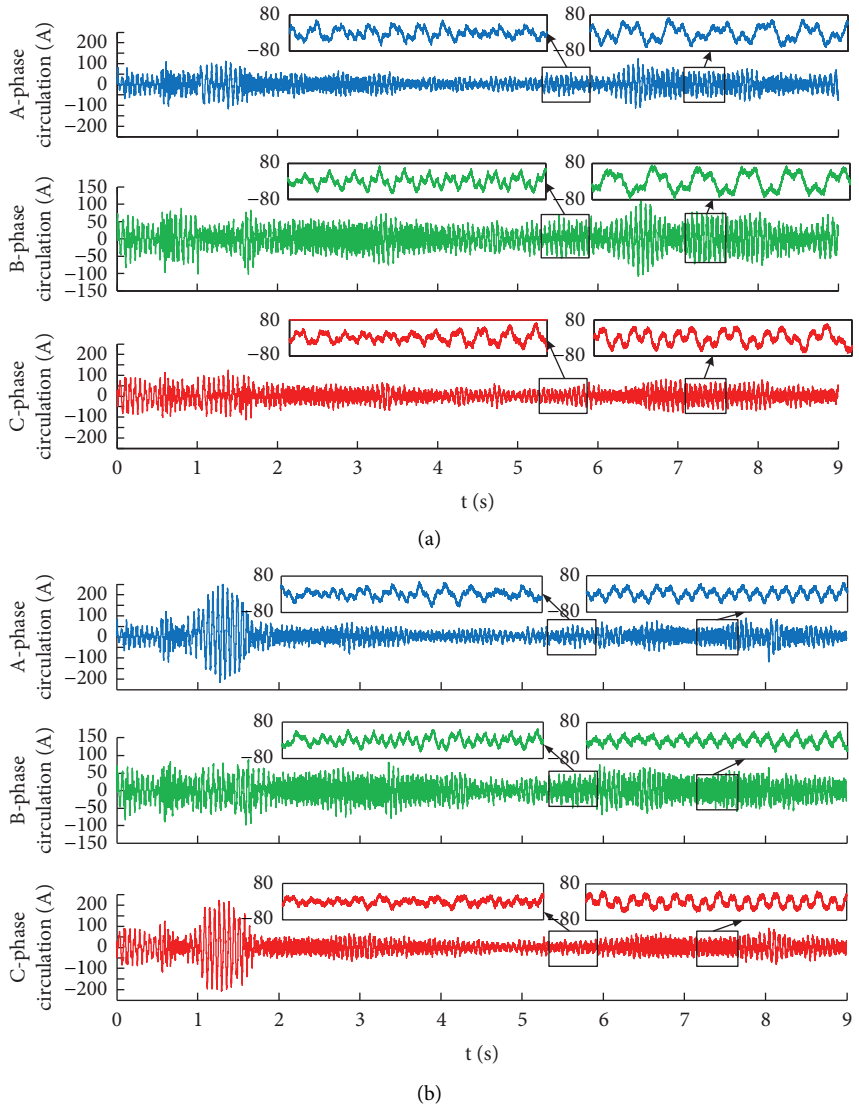

Figure 21: MMC-BESS three-phase circulation. (a) One-third average method, MMC-BESS three-phase circulation. (b) Sliding window integral method, MMC-BESS three-phase circulation.

three-phase circulation of *A*, *B*, and *C* using one-third average method were 123.3 A, 107.7 A, and 81.2 A, respectively. After the improvement, the maximum peak values of the three-phase circulation of *A*, *B*, and C using feedforward sliding window integral method were 85.83 A, 73.91 A, and 70.01 A, respectively.

Figure 22 shows the output power of three-phase battery: the DC load increased suddenly at 0.5 s. With the goal of stabilizing the DC bus voltage, the battery is discharged rapidly, and the maximum output power of the battery is 7.5×10^6 W. When the three-phase grid-side voltage was unbalanced, in order to compensate for the power difference

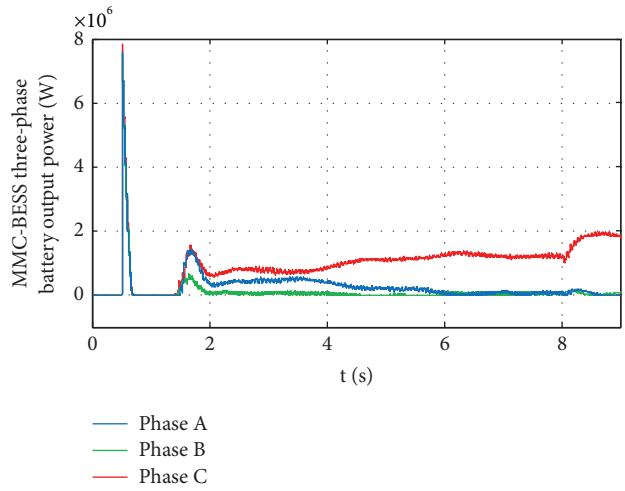

Figure 22: MMC-BESS three-phase battery output power.

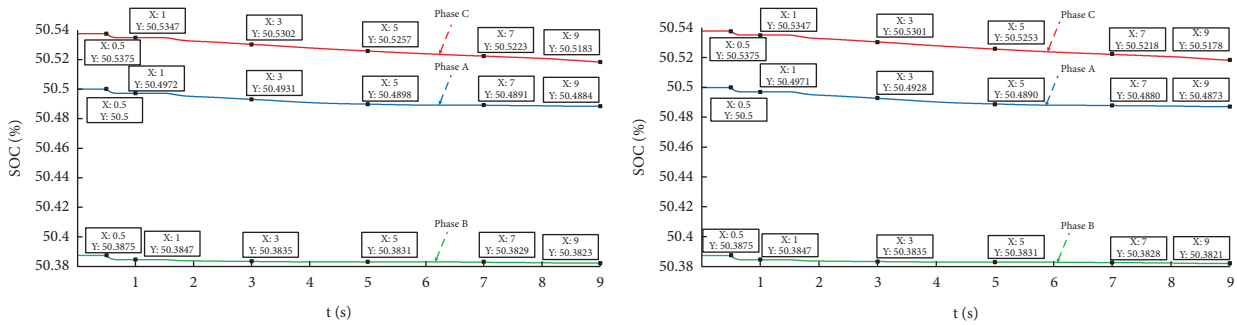

Figure 23: MMC-BESS three-phase SOC average. (a) One-third average method, three-phase SOC average. (b) Sliding window integral method, three-phase SOC average.

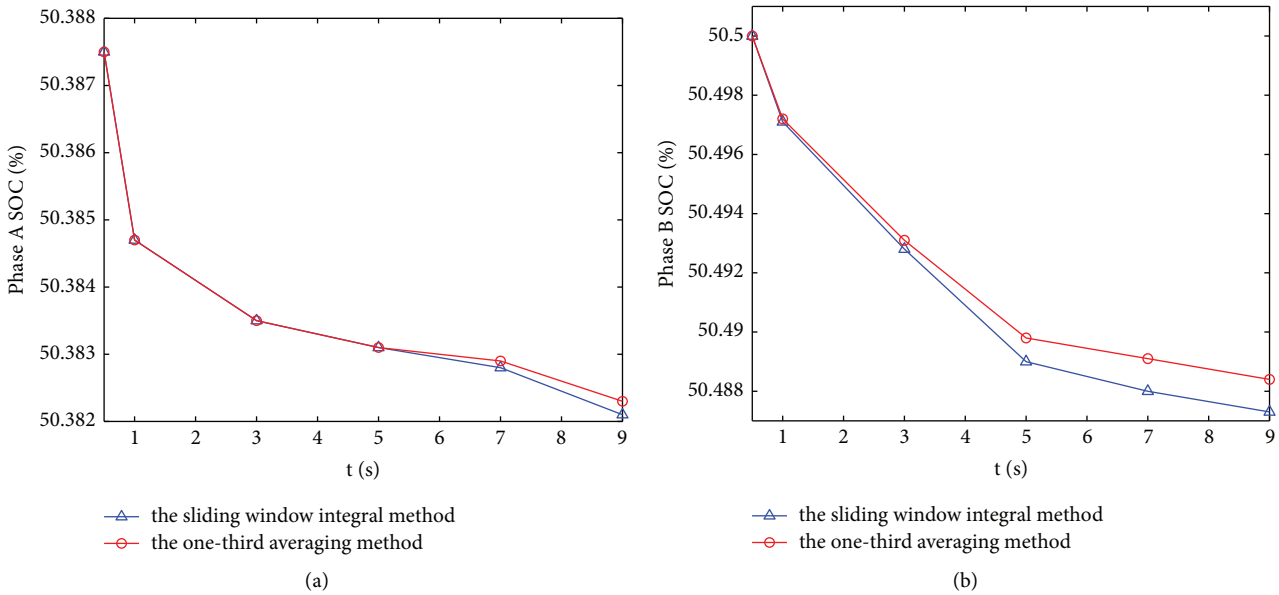

Figure 24: Continued.

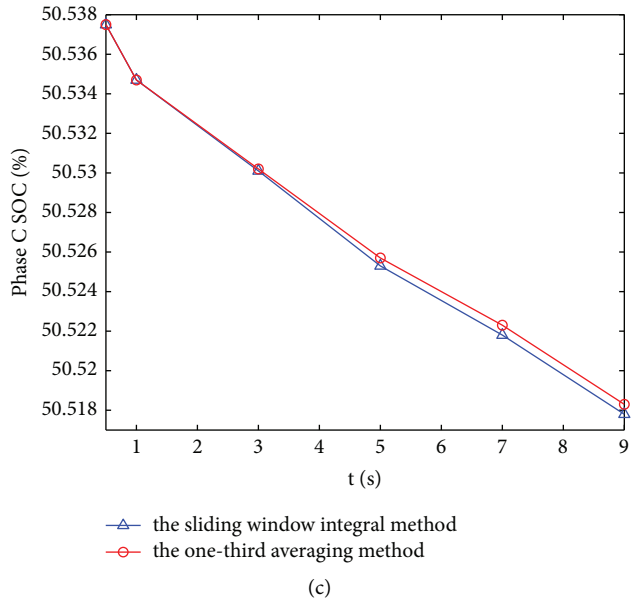

(c)

Figure 24: SOC average value of three phases of the MMC-BESS. (a) Sliding window integral method of phase *A*, SOC average using one-third average method. (b) Sliding window integral method of phase *B*, SOC average using one-third average method. (c) Sliding window integral method of phase *C*, SOC average using one-third average method.

Table 5: Comparison of SOC data between one-third average method and sliding window integral method.

Comparison of SOC data						
One-third average method:						
	0.5 s	1 s	3 s	5 s	7 s	9 s
Phase *A*	50.5000	50.4972	50.4930	50.4898	50.4891	50.4884
Phase *B*	50.3875	50.3847	50.3834	50.3831	50.3829	50.3823
Phase *C*	50.5375	50.5347	50.5302	50.5257	50.5223	50.5183
Sliding window integral method:						
	0.5 s	1 s	3 s	5 s	7 s	9 s
Phase *A*	50.5000	50.4971	50.4928	50.4890	50.4880	50.4873
Phase *B*	50.3875	50.3847	50.3835	50.3831	50.3828	50.3821
Phase *C*	50.5375	50.5347	50.5301	50.5253	50.5218	50.5178

among the three phases, the three-phase current can be quickly balanced. The lithium battery of the submodule of the MMC-BESS three-phase energy storage was continuously discharged, but the three-phase output was uneven. In order to quickly balance lithium battery of the SOC of each phase under the condition of uneven three-phase output and improve the utilization rate and service life of energy storage capacity, it was necessary to balance the SOC of the lithium battery of each energy storage submodule in the three phases of MMC-BESS.

In order to verify the effectiveness of the control strategy proposed in this paper, the system has been put into the three-level SOC equalization correction controller after a sudden change in DC load at 0.5 s. Figures 23 and 24 and Table 5 compare the equalization correction control proposed in this paper with the equalization correction control of the one-third average method. Under the same initial value of SOC, by comparing the results of the final SOC value of each phase at the same moment, it could be seen that the correction control proposed in this paper had a faster convergence and equalization speed. Using one-third average method, the initial values of the SOC of phases *A*, *B*, and *C* are 50.5000, 50.3875, and 50.5375, respectively; the final values of the SOC of phases *A*, *B*, and *C* are 50.4884, 50.3823, and 50.5183, respectively; the difference of the SOC of phases *A*, *B*, and *C* is 0.0116, 0.0052, and 0.0192, respectively. Using the sliding window integral method, the initial values of SOC of the phases *A*, *B*, and *C* are the same, and the final difference is 0.0127, 0.0054, and 0.0197, respectively.

5. Conclusion

In this paper, the characteristics of MMC-BESS phase unit power and the power difference between the upper and lower bridge arms are analyzed, a three-level SOC equalization correction control strategy is constructed, and a feedforward sliding window integral link is introduced into

the equalization correction control layer of the upper and lower bridge arms, so as to weaken the influence of the fundamental frequency AC circulating current and DC circulating current caused by the capacitor voltage fluctuation of the submodule on system. A three-phase 5-level MMC-BESS simulation model is built in the Matlab/Simulink environment. The results show that:

(1) When the DC load changes suddenly, or the three-phase network side voltage is unbalanced, the DC bus voltage has good stability, the maximum fluctuation is 1500 V, and the steady-state error is 7.5%;

(2) MMC-BESS has good compensation ability for three-phase network side current when the two-phase voltage drops by 50%. After compensation, the THD of three-phase current is 1.38%, and the unbalance degree is 2.4%. The system has strong robustness;

(3) The effectiveness of the three-stage SOC equalization correction control strategy with sliding window integral method proposed in this paper is verified, and the SOC of each phase lithium battery has a faster equalization convergence speed.

Data Availability

The datasets used and analyzed during the current study are available from the corresponding author upon reasonable request.

Conflicts of Interest

The authors declare that they have no conflicts of interest.

Acknowledgments

This work was supported by the scientific research project of the Shaanxi Provincial Department of Education, under Grant 17JK0337.

References

[1] Z. Y. He, "Discussion on harmonic hot issues of distributed new energy integration into power grid," *Southern Power Grid Technology*, vol. 10, no. 03, pp. 47–52+5, 2016.

[2] X. W. Ma, H. C. Xu, X. Liu et al., "A test method for the fast frequency response function of new energy stations in the northwest transmission-end large power grid," *Power grid technology*, vol. 44, no. 04, pp. 1384–1391, 2020.

[3] X. S. Tang and H. Y. Lu, "The influence of wind power flexible DC grid connection and frequency modulation control on power angle stability of power system," *Proceedings of the Chinese Society for Electrical Engineering*, vol. 37, no. 14, pp. 4027–4035+4281, 2017.

[4] J. L. Li, X. D. Yuan, Z. G. Yu, and L. Ge, "A review of research on using energy storage systems to improve power quality of power grids," *Automation of Electric Power Systems*, vol. 43, no. 08, pp. 15–24, 2019.

[5] N. Mukherjee Mukherjee and D. Strickland Strickland, "Analysis and comparative study of different converter modes in modular second-life hybrid battery energy storage systems," *IEEE Journal of Emerging and Selected Topics in Power Electronics*, vol. 4, no. 2, pp. 547–563, 2016.

[6] S. Wang, L. Jing, X. Z. Wu, J. Li, W. Wu, and J. Jiang, "Distributed control strategy for modular multi-level energy storage converters," *Automation of Electric Power Systems*, vol. 42, no. 12, pp. 113–121, 2018.

[7] L. Guo, H. Liang, and W. G. Zhang, "State-of-charge control strategy of battery energy storage system based on modular multilevel converter," *Power System Technology*, vol. 41, no. 08, pp. 2688–2697, 2017.

[8] I. Trintis, S. Munk-Nielsen, and R. Teodorescu, "A new modular multilevel converter with integrated energy storage," *IEEE Transactions on Industrial Electronics*, vol. 62, no. 2, pp. 1034–1046, 2011.

[9] Y. Chen, H. Wang, M. Zhu, M. Liu, J. Ma, and X. Cai, "Three-port modular multilevel converter based on hybrid sub-modules and full-leg inductance: simplified modeling and grid interconnection control strategy," *China Electrical Engineering Journal*, vol. 42, no. 5, 2021.

[10] S. Y. Li, T. Wu, B. Ren, Y. Xu, and C. Yuan, "Overview of energy storage systems based on modular multilevel converters," *Power System Protection and Control*, vol. 43, no. 16, pp. 139–146, 2015.

[11] A. A. Taffese, A. G. Endegnanew, S. D'Arco, and E. Tedeschi, "Power oscillation damping with virtual capacitance support from modular multilevel converters," *IET Renewable Power Generation*, vol. 14, no. 5, pp. 897–905, 2020.

[12] Q. Song, J. W. Meng, Y. B. Zhou, S. Xu, L. Yang, and K. Wang, "MMC's capacitor voltage ripple effect and its influence on the optimal design of converters [J/OL]," *Power Grid Technology*, vol. 45, no. 11, 2021.

[13] Q. Fan, X. B. Zhao, C. Y. Zhao, and J. Xu, "Adaptive fault current limiting control strategy for modular multilevel converters," *Automation of Electric Power Systems*, vol. 45, no. 17, pp. 126–133, 2021.

[14] Q. F. Yang, Y. B. Huang, M. X. Shi, J. Zhou, X. Chen, and J. Wen, "Distributed control method of multi-group optical storage units in DC microgrid based on consensus algorithm," *Proceedings of the Chinese Society for Electrical Engineering*, vol. 40, no. 12, pp. 3919–3928, 2020.

[15] Q. Chen, L. H. Zhang, Y. J. Wu, D. Gao, and Y. Zou, "Research on SOC equalization strategy of energy storage MMC converter," *Electrical Measurement and Instrumentation*, vol. 57, no. 05, pp. 37–43, 2020.

[16] N. Li, F Gao, T. Hao, Z. Ma, and C. Zhang, "SOH balancing control method for the MMC battery energy storage system," *IEEE Transactions on Industrial Electronics*, vol. 65, no. 8, pp. 6581–6591, 2018.

[17] J. I. Y. Ota, T. Sato, and H. Akagi, "Enhancement of performance, availability, and flexibility of a battery energy storage system based on a modular multilevel cascaded converter (MMCC-SSBC)," *IEEE Transactions on Power Electronics*, vol. 31, no. 4, pp. 2791–2799, 2016.

[18] T. Soong and P. W. Lehn, "Assessment of fault tolerance in modular multilevel converters with integrated energy storage," *IEEE Transactions on Power Electronics*, vol. 31, no. 6, pp. 4085–4095, 2016.

[19] M. Mao, Y. Ding, L. Chang et al., "Multi-objective power management for EV fleet with MMC-based integration into smart grid," *IEEE Transactions on Smart Grid*, vol. 10, no. 2, pp. 1428–1439, 2019.

[20] S. Wang, L. Jing, X. Z. Wu, and X. Zhao, "MMC-based SOC balance control of energy storage system," *Power Electronics*, vol. 50, no. 11, pp. 60–62+90, 2016.

[21] L. Zhang, F. Gao, and N. Li, "Control strategy of MMC battery energy storage system under asymmetrical grid voltage condition," *Chinese Journal of Electrical Engineering*, vol. 2, no. 2, pp. 76–83, 2016.

[22] H. B. Tao, X. F. Yang, Z. J. Li, Q. Zheng, X. You, and P. Kobrle, "MMC-based supercapacitor energy storage system and its improved SOC balance control strategy in electric energy routers," *Power System Technology*, vol. 43, no. 11, pp. 3970–3978, 2019.

[23] J. G. Li, W. B. Yang, Q. Song, Y. Huang, and W. Liu, "Distributed equalization control method of modular multilevel converter capacitor voltage," *Automation of Electric Power Systems*, vol. 40, no. 17, pp. 197–203, 2016.

[24] Y. L. Yu, Y. H. Xu, and X. B. Liu, "Harmonic current detection method of sliding window iterative DFT," *Power System Protection and Control*, vol. 39, no. 13, pp. 78–82+90, 2011.

[25] Y. N. Wang, C. Y. Guo, S. Yang, B. Pang, and X. Lin, "Non-monotonic variation characteristics and mechanism analysis of MMC system stability margin with inner loop current control bandwidth," *Proceedings of the Chinese Society for Electrical Engineering*, vol. 42, no. 10, 2021.